Journal of Experimental Botany, Vol. 61, No. 5, pp. 1293–1309, 2010
doi:10.1093/jxb/erq019 Advance Access publication 4 March, 2010

Journal of Experimental Botany
www.jxb.oxfordjournals.org

DARWIN REVIEW

Terrestrial plant production and climate change

Andrew D. Friend*

Department of Geography, University of Cambridge, Downing Place, Cambridge CB2 3EN, UK

*E-mail: adf10@cam.ac.uk

Received 19 August 2009; Revised 8 January 2010; Accepted 15 January 2010

Abstract

The likely future increase in atmospheric CO_2 and associated changes in climate will affect global patterns of plant production. Models integrate understanding of the influence of the environment on plant physiological processes and so enable estimates of future changes to be made. Moreover, they allow us to assess the consequences of different assumptions for predictions and so stimulate further research. This paper is a review of the sensitivities of one such model, Hybrid6.5, a detailed mechanistic model of terrestrial primary production. This model is typical of its type, and the sensitivities of the global distribution of predicted production to model assumptions and possible future CO_2 levels and climate are assessed. Sensitivity tests show that leaf phenology has large effects on mean C_3 crop and needleleaved cold deciduous tree production, reducing potential net primary production (NPP) from that obtained using constant maximum annual leaf area index by 32.9% and 41.6%, respectively. Generalized Plant Type (GPT) specific parameterizations, particularly photosynthetic capacity per unit leaf N, affect mean predicted NPP of higher C_3 plants by –22.3% to 27.9%, depending on the GPT, compared to NPP predictions obtained using mean parameter values. An increase in atmospheric CO_2 concentrations from current values to 720 ppm by the end of this century, with associated effects on climate from a typical climate model, is predicted to increase global NPP by 37.3%. Mean increases range from 43.9–52.9% across different C_3 GPTs, whereas the mean NPP of C_4 grass and crop increases by 5.9%. Significant uncertainties concern the extent to which acclimative processes may reduce any potential future increase in primary production and the degree to which any gains are transferred to durable, and especially edible, biomass. Experimentalists and modellers need to work closely together to reduce these uncertainties. A number of research priorities are suggested.

'*The green leaf or, to be more precise, the microscopic green grain of chlorophyll, is the focus, the point in the world to which solar energy flows on one side while all the manifestations of life on earth take their source on the other side.*'
Kliment Arkadievich Timiryazev *The conclusions of a century of plant physiology, speech at Moscow University, 12 January 1901*

Key words: Climate change, CO_2, GPP, model, NPP, photosynthesis, production.

Introduction

The productivity of land plants provides humans with the bulk of their food and fibre and strongly influences the dynamics of atmospheric CO_2. Quantifying and explaining the current global distribution of plant production, and predicting its future responses to climate change and increasing atmospheric CO_2, are therefore major scientific objectives. This paper is a review of current approaches to modelling global plant production, and looks in detail at the parameterizations and sensitivities of a global-scale mechanistic model, Hybrid6.5, to illustrate typical abilities, findings, and remaining challenges in this area of research.

Major advances in our ability to simulate the global distribution of photosynthesis, plant production, and their dynamics have occurred over the last two decades. Improvements in physiological and biophysical understanding, model approaches, validation and calibration measurements, forcing datasets, and computer power have increased

Abbreviations: GCM, global climate model; GPT, generalized plant type; GPP, gross primary production; LAI, leaf area index; NPP, net primary production; PAR, photosynthetically active radiation; PEPCase, phosphoenolpyruvate carboxylase; RuBP, ribulose 1-5 *bis*phosphate.

model rigour, accuracy, and spatial resolution. The utility of models lies not only in their absolute predictions, but at least as importantly in their ability to identify relationships between our level of understanding of individual processes and the quantity of interest. In other words, knowledge generated as a result of continual model development and appraisal helps to structure research priorities efficiently.

Mechanistic models of plant production allow us to address a wide range of interesting questions; some examples might include: How important are physiological differences between plant species in comparison to environmental variability for ecosystem processes? What proportion of plant production enters the human food chain, and how is this proportion spatially distributed? To what extent does soil surface evaporation reduce global productivity? Are leaf area dynamics in some sense optimal? Are the ultimate constraints on productivity environmental or biological? How have gymnosperms managed to persist despite more primitive physiology than angiosperms? How was plant production distributed spatially at various times in the past, and how might it change in the future? What role might acclimative processes play in determining future global primary production? A selection of these questions are addressed here as examples of the utility of plant production models.

Global plant production models

Models of global plant production vary from highly aggregated empirical approaches (e.g. Prince and Goward, 1995), to complex mechanistic representations of coupled biology and physics (e.g. Bonan *et al.*, 2003). Predicting the impacts of climate change and increasing atmospheric CO_2 requires a relatively sophisticated approach to surface physics (e.g. radiation transfer, soil hydrology, surface temperature, and atmospheric coupling), as well as detailed mechanistic treatments of physiological (e.g. photosynthesis responses to light, CO_2, temperature, and N content, integration to the whole canopy, acclimation, species-specific physiologies, respiration, growth, allocation, and phenology) and ecological (e.g. regeneration, mortality, nutrient feedbacks, competition, and impacts of disease, herbivory, pollution, and management) processes.

An important distinction between mechanistic approaches to modelling whole plant photosynthesis concerns the treatment of photosynthetic capacity and scaling of photosynthesis over the canopy volume. Photosynthetic capacity in this context is the metabolic potential for photosynthesis on a unit ground area basis. This quantity is determined by the chloroplast enzyme and chlorophyll content, and its distribution over the canopy. Some models prescribe capacity (e.g. CASA: Potter *et al.*, 1993), whereas others predict the dynamics of leaf area (e.g. LPJ: Sitch *et al.*, 2003) and canopy N content (e.g. O-CN: Zaehle and Friend, 2010). Scaling photosynthesis over the canopy is often achieved assuming linearity between the rate of net photosynthesis and absorbed radiation (the so-called 'big leaf' approach; Sellers *et al.*, 1992; often justified on the grounds of optimal distribution of photosynthetic capacity, but see Friend, 2001). However, a more accurate approach is explicitly to integrate over canopy sub-volumes with spatially varying physics and physiology (e.g. O-CN: Zaehle and Friend, 2010).

A mechanistic model of plant production can be logically broken down into three distinct components: external forcing, physical processes, and biological processes. External forcing typically consists of climate and soil variables, whose space and time scales will determine the simulation domain and resolution. Physical processes may consist of radiation transfer, water flows and state transitions, and the dynamics of heat. Biological processes may consist of canopy net photosynthesis, mitochondrial respiration in non-foliage tissues, nutrient uptake, allocation and growth, and litter turnover. They may also include mortality and regeneration (e.g. Hybrid4.1: Friend and White, 2000), or at least a parameterization of competition processes, for example, using Lotka–Volterra equations based on relative productivity (e.g. TRIFFID: Cox, 2001).

Model predictions

Global plant production is usually expressed in terms of annual net primary production, NPP. NPP is the annual increment in plant dry mass after allowing for losses due to respiration of CO_2, but before any litter losses. Although NPP is a measure of dry matter increment, the conservative stoichiometry of plant tissues make it convenient to express NPP in purely carbon, e.g. or CO_2 units (it is often assumed that dry matter is 45% carbon, e.g. Leith, 1973).

The first known published estimate of global terrestrial plant production, based on field measurements, was that of Eberymayer in 1881 (cited in Leith, 1973), who extrapolated from measurements in Bavarian forests and croplands to arrive at a global figure of 90 Pg (1 Pg=10^{15} g) CO_2 yr^{-1}. The many different estimates over subsequent years reflect uncertainty in areal extent of different vegetation types and their classification, as well as mean rates of production. Modern estimates began with the work of Whittaker, Likens, and Leith during the seminal International Biological Program (1964–1974). For example, Leith (1973) calculated global NPP during the 1950s to be 100.2 Pg DM yr^{-1} (equivalent to 45.1 Pg C yr^{-1}, assuming 0.45 g C g^{-1} DM), based on a compilation of productivity data for different vegetation types and estimates of their areal coverage. More recently, Field *et al.* (1998) published a mean value of 56.4 Pg C yr^{-1} for calendar years 1982–1990, based on the CASA production efficiency model, constrained by satellite measurements of light absorption. Modern published estimates range 36–74 Pg C yr^{-1}, depending on the method employed (Cramer *et al.*, 1999; Zaks *et al.*, 2007).

A new highly mechanistic global model of photosynthesis is used in this paper to investigate the relationships between current understanding and predictions of the distribution of plant production over the Earth's land surface. The model is then used to estimate the possible distribution of plant production at the end of this century given increased

concentrations of atmospheric CO_2 and associated changes in climate patterns.

Methods

The model: Hybrid6.5

Hybrid6.5 simulates the carbon, nitrogen, phosphorus, water, and energy fluxes and structural changes in terrestrial ecosystems at hourly to decadal timescales, and at spatial scales ranging from the individual plant to the whole Earth. The main sub-models treat: (i) canopy photosynthesis and stomatal conductance; (ii) respiration and partitioning of labile C to various tissues and uptake and partitioning of labile N and P; (iii) litter production; (iv) soil organic matter decomposition; (v) canopy radiation transfer; (vi) surface energy and water balance; and (vii) height structured competition between individuals in plots. Soil properties such as water-holding capacity are prescribed. Climate forcing can be provided by mean-monthly climate data (downscaled to sub-hourly timesteps using a weather generator), or through coupling to a model of the atmosphere such as a global climate model (GCM).

A baseline simulation of global plant production was performed and is presented here. This simulation was designed to provide the most accurate estimate currently possible and was achieved by coupling current understanding of the physiology of photosynthesis with the best available forcing datasets. In order to constrain the estimate using observations as far as possible, the distributions of plant types, leaf areas, and photosynthetic capacity per unit leaf area were prescribed from remote sensing and *in situ* observations (see below), rather than modelled prognostically as in the fully dynamic implementation of the model.

Hybrid6.5 differs from previously published versions of the Hybrid model (described in Friend and White, 2000, and references therein) in a number of ways. Those differences most relevant for the simulations presented here are: (i) canopy physiology and photosynthetic capacity in C_3 plants are as in the canopy model of Friend and Kiang (2005); (ii) canopy physiology and photosynthetic capacity in C_4 plants are as described below; (iii) a 30 min timestep is used for all calculations, rather than a daily timestep; (iv) the optimal temperature for chloroplast electron transport acclimates to the prevailing conditions (see below); and (v) surface physics are modelled using an implementation of a GCM land surface scheme, treating explicitly separate patches of different vegetation types within each land surface climate grid box. In addition, because the distributions of plant types and leaf area are prescribed, in order not to confound the results unnecessarily the parameterizations of physiological damage from frost or drought were switched off (these parameterizations are important for determining the outcome of competition, but are presumed less critical under the constraints imposed here). Processes such as growth and allocation are not implemented for these simulations. Details of how the physiology is treated that are relevant to the simulations shown here are given below, and the relationships between the main parameters, variables, and other calculated quantities related to the calculation of NPP are described schematically in Fig. 1.

Leaf-level net photosynthesis: Photosynthesis in Hybrid6.5 is calculated using considerable physiological detail, and is based on the analytical solution to the leaf photosynthesis model of Kull and Kruijt (1998; hereafter KK),

$$A = \left(1-\frac{\Gamma^*}{C_\mathrm{i}}\right)[m_\mathrm{sat}N_\mathrm{sat}+\alpha m_1(1-r_\mathrm{r})I_0(e^{-k_a n_3 N_{sat}}-e^{-k_a n_3 N_p})] \quad (1)$$

where A is the instantaneous rate of whole leaf gross (i.e. not including mitochondrial respiration, but including photorespiration) photosynthesis on a leaf area basis, Γ^* is the photorespiration compensation point (in the absence of dark respiration), C_i is the intercellular CO_2 concentration, m_sat is the N-normalized rate of light-saturated carboxylation, N_sat is the cumulative leaf N content at which limitation by light harvesting takes over from limitation by Rubisco or maximum electron transport capacity, α is the intrinsic quantum efficiency for CO_2 uptake, m_1 is the ratio of electron transport limited carboxylation to maximum electron transport capacity limited carboxylation, r_r is leaf reflectance, I_0 is incident photosynthetically active radiation (PAR), k_a is the coefficient of PAR extinction on chlorophyll, n_3 is the ratio of chlorophyll to N (assumed constant through the leaf), and N_p is total leaf N on a leaf area basis.

Equation 1 differs from classical implementations of the 'Farquhar *et al.*' model of C_3 leaf photosynthesis (Farquhar *et al.*, 1980; von Caemmerer and Farquhar, 1981), such as those of Collatz *et al.* (1991) and Harley *et al.* (1992), in several important ways. It treats explicitly the extinction of light over chlorophyll through the leaf, thereby separating the leaf cross-section into a region of light saturated and a region of light harvesting limited chloroplasts. The rate of photosynthesis in the light saturated region is given by $\left(1-\frac{\Gamma^*}{C_\mathrm{i}}\right)m_\mathrm{sat}N_\mathrm{sat}$ and, as in the Farquhar *et al.* model, is limited by either electron transport capacity or the RuBP saturated rate of carboxylation. The rate in the light harvesting limited region is given by the remaining terms in Equation 1, and is linearly proportional to the amount of light absorbed in that region $\left[\text{i.e. } I_0\left(e^{-k_a n_3 N_\mathrm{sat}}-e^{-k_a n_3 N_\mathrm{p}}\right)\right]$. At low light the entire leaf may be light harvesting limited; conversely, if the chloroplast content is sufficiently low, the leaf may be entirely light saturated. The separation of regions within the leaf is calculated on each timestep as a function of incident light, temperature, C_i, and leaf N.

As well as resulting in more realistic relationships between incident light, photosynthetic capacity, and photosynthesis, this approach obviates the need for two empirical constants: a 'convexity' parameter describing the relationship between actual and potential rates of electron transport (e.g. Equation A 11 in von Caemmerer and Farquhar, 1981), and a parameter describing the smoothing between carboxylation and RuBP regeneration limited rates of photosynthesis

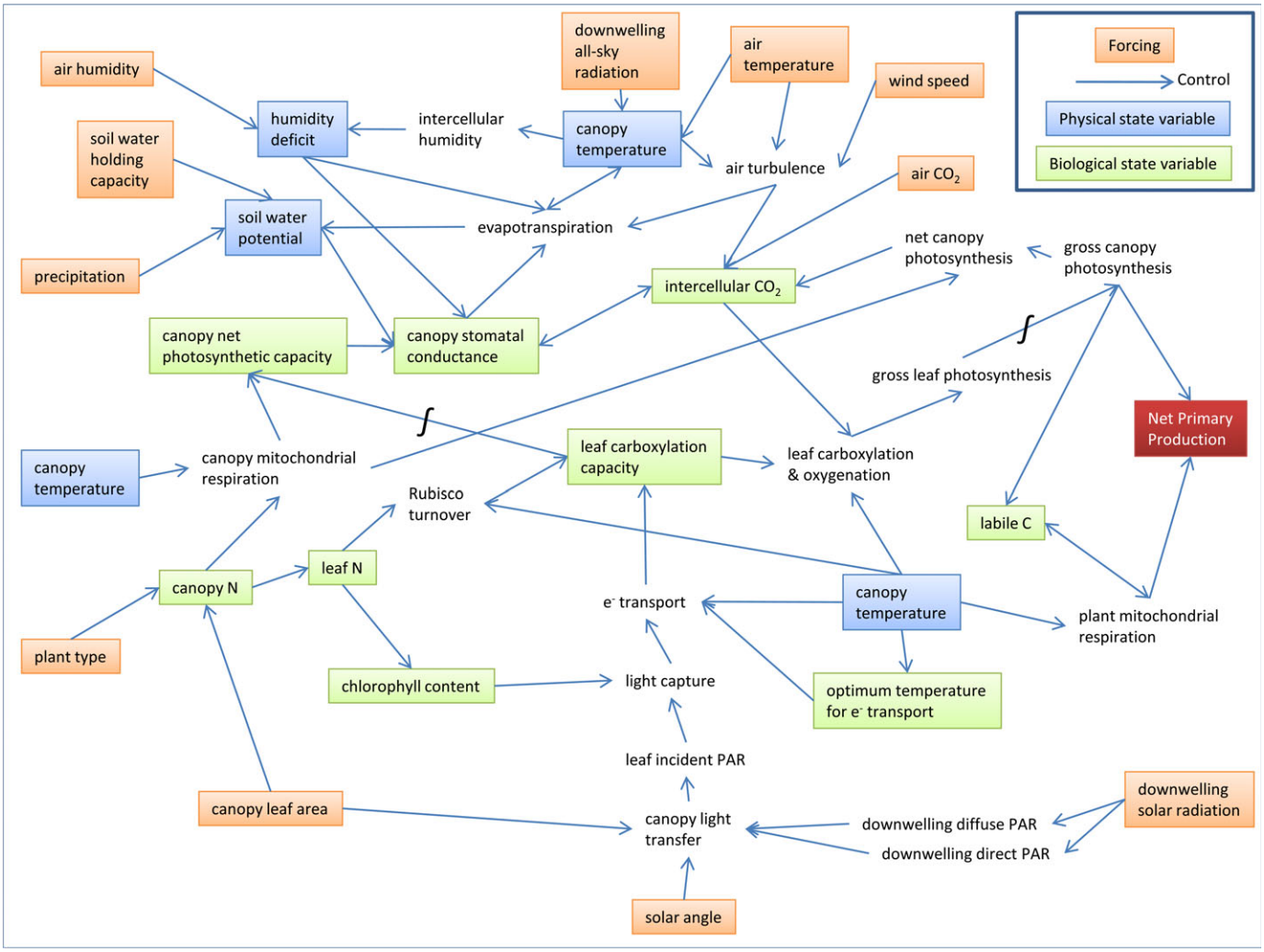

Fig. 1. Overview of relationships between forcing variables, state variables, and derived quantities related to the calculation of net primary production in the Hybrid6.5 model. The main quantity calculated is the rate of gross leaf photosynthesis. Leaf-level quantities are integrated to the canopy level. Canopy net photosynthetic capacity is the CO_2-saturated rate of canopy net photosynthesis. For clarity, only the top representation of canopy temperature (linked to evapotranspiration) shows its full derivation. See main text for full details of model structure.

(e.g. θ in Collatz *et al.*, 1991). Friend (1995) found that modelled net photosynthesis was more sensitive to this empirical smoothing parameter than any other model parameter, significantly compromising the mechanistic basis of the traditional approach and reducing its predictive ability. Also, Sands (1996) found strong sensitivity of canopy photosynthesis to the leaf-level convexity parameter. Additional evidence for the advantages of the KK approach compared to the traditional approach was provided by Friend (2001), and its superior predictive ability when scaled to the canopy level has been confirmed in comparisons with *in situ* flux data from a wide range of forest types (S Zaehle, personal communication).

The KK model of C_3 leaf photosynthesis was adapted for C_4 photosynthesis for the simulations performed here. Although C_4 leaf anatomy is different from that of C_3 leaves, the overall approach to separation of regions of light saturated and regions of light harvesting limited chloroplasts due to light extinction is assumed to hold. The KK model was adapted to C_4 metabolism using insight from the full intercellular C_4 transport (ICT) model of Collatz *et al.* (1992).

The KK model was adapted for C_4 physiology by adding an additional potential limitation to carboxylation due to the velocity of the phosphoenolpyruvate carboxylase (PEPCase) reaction in light saturated regions. This rate depends on the air space concentration of CO_2 and the activity of PEPCase, and the following equation was fitted to the ICT model,

$$msat_p = k n_f p_i / P \quad (2)$$

where $msat_p$ is the CO_2 limited N-specific rate of light saturated carboxylation (cf. Equation 1), k is a rate constant, n_f is the fraction of leaf N allocated to photosynthetic compounds, p_i is the air space partial pressure of CO_2, and P is total air pressure. k was calculated from the full ICT model to be 2 mol_{CO_2} mol^{-1} N s^{-1}, and is assumed to have a Q_{10}=2 temperature dependency as in Collatz *et al.* (1992). Within light saturated bundle sheath cells, the

potential limitations to C_3 photosynthesis due to electron transport capacity or RuBP saturated carboxylation are calculated as in a KK model, except that the CO_2 partial pressure is fixed at 7800 Pa, a value calculated using the full ICT model under peak rates of photosynthesis.

As in the C_3 KK model, the rate of photosynthesis in the light harvesting limited region is assumed to be a linear function of the rate of light absorption. However, the intrinsic quantum yield is reduced by 40% to account for the fraction of absorbed light assumed to be used for the PEPCase reactions (Berry and Farquhar, 1978).

In Hybrid6.5, the N-specific potential rate of carboxylation in both C_3 and C_4 leaves is assumed to fall with falling soil water potential, as indicated from combined *in situ* and modelling analysis of the response of tree canopy photosynthesis to drought (Keenan *et al.*, 2009). The functional form of this relationship is assumed to be a linear reduction down to the complete cessation of carboxylation at a soil water potential of –1.5 MPa.

It has been frequently observed that photosynthesis acclimates to growth temperature, although this plasticity is quite variable between species (Berry and Björkman, 1980). An important mechanism for temperature acclimation is believed to be change in the optimum temperature for photosynthetic electron transport, at least in winter wheat (Yamasaki *et al.*, 2002), although it is clear that a number of other factors also contribute to the temperature acclimation of photosynthesis (Hikosaka *et al.*, 2006). In order to examine the potential importance of this type of acclimation for the distribution of plant production, and its response to climate change, a straightforward parameterization was implemented in Hybrid6.5, and applied to all plant types. The temperature dependence of electron transport is modelled using the formulation suggested by June *et al.* (2004),

$$J(T_L) = J(T_o) e^{-\left(\frac{T_L - T_o}{\Omega}\right)^2} \quad (3)$$

where $J(T_L)$ is the rate of electron transport at leaf temperature T_L, $J(T_o)$ is the rate at the optimum temperature T_o, and Ω is an empirical parameter controlling the slope of the response either side of the optimum temperature, and is given here the value of 18 °C, the mean of the values observed by June *et al.* (2004) in soybean. June *et al.* (2004) explain why previous formulations of the response of photosynthetic electron transport to temperature were inaccurate, particularly in their prediction of more rapid declines above than below the optimum temperature, a feature not observed in whole intact leaves.

The optimum temperature for electron transport is assumed to decay towards an equilibrium optimum value during daylight hours,

$$\frac{dT_o}{dT} = -\lambda(T_o - T_e) \quad (4)$$

where T_e is the equilibrium optimum temperature (°C), and the decay constant $\lambda = -3.3\times10^{-6}$ s, giving an e-folding time of 3 d, based on evidence of rapid adjustment in many species (Veres and Williams, 1984). Rather than simply setting T_e to the prevailing canopy temperature, which may vary quite widely during the day, an optimal relationship was derived. A linear function between T_e and T_L was assumed, and the equation $17.0+0.35T_L$ (T_L in °C, daylight hours only) was found to maximize annual GPP in a broad-leaved deciduous forest in Pennsylvania, USA. It is encouraging to note that the slope of this relationship is very close to that observed in a range of plant species (studies cited by Hikosaka *et al.*, 2006). As a first approximation this relationship is assumed to hold everywhere, although it is recognized that different locations may require different coefficients for local optimality (this is tested, see below).

Canopy-level photosynthesis and respiration: Leaf-level photosynthesis is scaled to the canopy as described in Friend (2001) and Friend and Kiang (2005). A significant feature of the KK model is that light extinction over chloroplasts, and rates of photosynthesis, are both expressed on a leaf N basis. This greatly facilitates scaling from leaf to canopy and the parameterization of different plant species and plant types. Leaf N is assumed to fall exponentially down through the canopy with an extinction coefficient over cumulative LAI of –0.11. The ratio of chlorophyll to leaf N is assumed to increase with canopy depth according to the parameterization given by Friend and Kiang (2005), fitted to the field measurements of Kull and Kruijt (1998). This spatial variability in leaf physiology determines the photosynthesis–light response curves at different canopy depths and the bulk response curve of the entire canopy ('bulk' in this context refers to the effective value for mass flux across the total canopy surface on a ground area basis).

Leaf-level photosynthesis is summed over sunlit and shaded fractions in horizontal canopy layers of 0.5 LAI units deep, and then summed over layers to give canopy-level gross photosynthesis. Canopy respiration is then subtracted to give net canopy photosynthesis. Canopy respiration is calculated as a function of N content, temperature, and a plant type specific photosynthetic N scalar (see below). Respiration is given different N and temperature dependencies in C_3 and C_4 canopies (Friend *et al.*, 2009).

Canopy stomatal conductance and intercellular CO_2: Stomatal conductance is calculated directly at the bulk canopy level, and used to calculate a bulk canopy C_i for the photosynthesis calculations in each canopy layer. Canopy stomatal conductance is also used to calculate evapotranspiration (see below). The canopy stomatal conductance formulation is semi-empirical and includes dependencies on C_i, the leaf to air specific humidity gradient, soil water potential, and the potential rate of canopy photosynthesis under conditions of saturating CO_2. This last factor accounts for the stomatal dependencies on light, temperature, and photosynthetic capacity (see Friend and Kiang, 2005, for the rationale behind this approach). Parameter values in the conductance formulation are assumed to be

invariant over plant types, although this is almost certainly a significant approximation. However, determining plant type specific values would be a major undertaking, and sensitivity tests can be used with the present approach to determine those parameters, processes, and regions where plant type specific differences matter. Processes likely to play important roles in future responses to climate change include stomatal closure with increasing CO_2 concentrations, and responses to changing specific humidity. The empirical equation for the CO_2 response is,

$$f_{CO_2} = \frac{C_i + 0.004}{5C_i} \quad (5)$$

where f_{CO_2} is the relative effect of C_i on conductance, and the empirical constants were fitted to the data of Forstreuter (1998) for European beech. The relative response to specific humidity is,

$$f_\Delta = 2.8^{-80\Delta} \quad (6)$$

where f_Δ is the relative effect of specific humidity deficit on conductance, and Δ is the specific humidity deficit between the internal leaf air spaces and the external leaf surface ($kg_{(water\ vapour)}\ kg^{-1}_{(air)}$). The empirical constants were determined as described in Friend and Kiang (2005), and give a strong closing response.

Whole plant mitochondrial respiration and growth: NPP is taken as the difference between canopy gross photosynthesis and whole plant mitochondrial respiration (R_m). R_m is assumed to be substrate limited, and is therefore proportional to the size of a labile carbon pool,

$$R_m = f_{T,Rm} k_m M_{C,l} \quad (7)$$

where $f_{T,Rm}$ is a temperature response function, k_m is a constant of proportionality, and $M_{C,l}$ is plant labile C mass. The temperature response function is assumed to be an Arrhenius-type function, with constants calibrated to give an overall Q_{10} response of 2 around 10 °C; i.e. $7.65\times10^7 e^{-45000/RT_L}$, where R is the universal gas constant (respiration is assumed to be proportional to canopy temperature, which in the simulations presented here is set to the upper soil layer temperature; see below).

The time derivative of the labile C pool is given by,

$$\frac{dM_{C,l}}{dt} = U_C - R_m - G_C \quad (8)$$

where U_C is canopy photosynthesis and G_C is the rate of incorporation of labile C into structural tissues. The labile C pool is assumed to have a turnover time of 14 d, a value reflecting evidence across a range of studies (references cited by Bowling *et al.*, 2008). It is also assumed that, over a sufficient length of time, respiration accounts for half of the labile C turnover, the other half going to growth (experimental support for the constancy of this ratio is given by Gifford, 1995), and therefore $k_m = 0.5/\tau_{Cl}$, where τ_{Cl} is the turnover time of the labile pool. G_C is calculated in the same way as R_m (with equal parameter values) in the simulations presented here (the fully dynamic implementation of the model calculates G_C as a function of demand for labile C by meristems). Therefore the details of the temperature response function, such as its Q_{10} value, do not affect NPP or respiration over sufficiently long time periods, such as a year.

Light, heat, and water: The distributions of direct and diffuse PAR over the canopy are modelled following the approach of Spitters (1986), as described by Friend (2001). PAR extinction over leaf area is based on extinction over canopy layers, but treats the separate profiles of direct and diffuse irradiances, and the scattering of direct PAR which increases the diffuse flux at lower levels.

Surface heat and water fluxes are modelled using an implementation of the NASA Goddard Institute for Space Studies (GISS) global climate model (GCM) II (Hansen *et al.*, 1983) as described by Friend *et al.* (2009). Two soil layers (an upper of 0.1 m and a lower of 4 m thickness) are treated, with heat and water content followed in each. For the purposes of energy balance and temperature, the upper layer is assumed to include all vegetation structure as well as the actual soil. The heat content of this upper layer varies with the balance of inputs from absorbed solar radiation and heat in precipitation, and losses to net upward longwave radiation, sensible and latent heat fluxes, and net transfer with the lower layer. Canopy temperature is assumed to be equal to the temperature of the upper soil layer. The flux of heat between the upper and lower soil layers depends on their relative temperatures and a thermal conductivity parameter. The upper layer soil water is modelled as a function of inputs from precipitation, and outputs to transpiration, bare soil evaporation, run-off, and the net flux with the lower layer. Transpiration is assumed to come from the soil layer with the highest relative water content to which the plant has access. Fluxes of heat, moisture, and CO_2 from the surface to the atmosphere are calculated using a drag law parameterization (Hansen *et al.*, 1983; Friend and Kiang, 2005).

Atmospheric forcing: Climate and CO_2 forcing is assumed to be located at a level 10 m above the top of the canopy. A stochastic daily weather generator based on the WGEN model of Richardson and Wright (1984) and the SIMMETEO model of Geng *et al.* (1988) is used (Friend, 1998). This approach employs a first-order Markov chain and associated dependencies to down-scale mean-monthly precipitation, number of wet days, 24 h maximum and minimum temperatures, radiation, and vapour pressure to daily values of precipitation, maximum and minimum temperature, downwelling radiation (shortwave, direct and diffuse PAR, and longwave), and specific humidity to daily values. Daily values are created for one month, and then adjusted such that the monthly mean is equal to the mean-monthly value in the forcing. This ensures that each annual climate cycle is identical to the prescribed forcing, reducing the time to equilibrium when using a mean climatology, but maintaining realistic variation between days in each month. Radiation and air temperature are then distributed across

sub-daily timesteps using the daytime progression of sun angle (Friend *et al.*, 2009). The daily ratio of actual to potential shortwave radiation is used to calculate the daily cycle of direct and diffuse PAR using the relationships given by Spitters *et al.* (1986). Atmospheric pressure is assumed fixed at 101 325 Pa and wind speed at 2 m s^{-1}.

Plant type parameters: To allow treatment of global scale variation in important plant physiological properties, species are classed into nine 'Generalized Plant Types' (GPTs). GPT specific parameter values are given in Table 1, and their derivation is described in Friend and Kiang (2005) and Friend *et al.* (2009). In the simulations presented here it is assumed that the first order physiological differences between leaves of C_3 plants are accounted for by differences in total N (this is a prognostic variable in the fully dynamic implementation of Hybrid6.5), the fraction of N allocated to photosynthetic compounds (n_f), and specific leaf area. The KK model of leaf photosynthesis includes proportionality constants relating maximum electron transport rate (J_{max}) and maximum potential carboxylation ($V_{c,max}$) to leaf N. These values are both calibrated for different GPTs using a relative photosynthetic capacity parameter (Table 1). Most GPT parameter values were taken from the literature, but flux tower data were used to estimate the ratios of photosynthetic capacity to foliage N and the canopy conductance parameters.

Implementation: Atmospheric forcing above the plant canopy and/or bare soil is assumed to apply to a whole grid box, with sides of 0.25° latitude and longitude. Each grid box is divided into separate surfaces, each with a different vegetation cover or with bare soil. Surface physics are calculated separately for each surface, allowing soil moisture contents and temperatures to evolve independently. Surfaces can contain many individuals of different GPTs. However, here a single fixed-size individual is simulated on each vegetated surface, with the number of vegetated surfaces in each grid box equal to the number of GPTs assigned from a land cover dataset (see below). To obviate confounding effects of growth on NPP, canopy height and rooting depth are both fixed at 1 m for all individuals (these properties have only a small effect on canopy conductance and ensure access to water in all soil layers). The absolute size of the individual is otherwise not relevant for the simulations presented here. An integration timestep of 30 min is used, but the hydrology and energy flux calculations switch to a shorter timestep if necessary to ensure numerical stability.

Forcing data for the baseline simulation

Datasets describing the global distributions of terrestrial vegetation characteristics (i.e. plant type and monthly leaf area), soil structure (i.e. available water storage capacity), and land surface climate (i.e. monthly precipitation, number of wet days, temperature, radiation, and vapour pressure) were processed into formats suitable as inputs to the model. Climate and leaf area datasets are available as time-series, and the monthly mean values for calendar years 2001–2006 were used for consistency between forcings. All global fields were formatted to a common 0.25×0.25° (QD) resolution latitude×longitude grid covering all land areas except Antarctica. The concentration of atmospheric CO_2 was prescribed as a single global value, and vegetation parameters were prescribed for each plant type. Further details on how these datasets were used are given below.

Plant types: The global distribution of the fractional cover of GPTs was assumed fixed and was derived from the IGBP DISCover land cover datasets. These data are based on satellite observations, and were derived using 1 km monthly Advanced Very High Resolution Radiometer Normalized Difference Vegetation Index composites covering calendar years 1992–1993, as described by Loveland *et al.* (2000). Fractional cover datasets, already aggregated to QD resolution, were downloaded from http://islscp2.sesda.com

Table 1. Generalized plant type (GPT) mnemonics and leaf physiology parameter values

C4GR uses the C_4 photosynthetic pathway, with intrinsic quantum yield=0.05 mol CO_2 mol^{-1} quanta; all other plant types use C_3 physiology with intrinsic quantum yield=0.08 mol CO_2 mol^{-1} quanta. Relative photosynthetic capacity is with respect to the values given by Kull and Kruijt (1998) for the ratios of maximum chloroplast electron transport rate and maximum rate of carboxylation to total leaf N. Derivation of parameters is described in Friend *et al.* (2009) and Friend and Kiang (2005). The mean GPT is used for a sensitivity test of the model (SIM4), and has the mean parameter values across the non-moss C_3 GPTs.

Mnemonic	Full name	Specific leaf area (m^2 kg^{-1} C)	Mean foliage N (% DM)	Relative photosynthetic capacity –	Minimum stomatal conductance (mm H_2O s^{-1})	Maximum stomatal conductance (mm H_2O s^{-1})
BREVt	Broadleaved evergreen tree	18	1.8	1.1	0.1	5
BRDDt	Broadleaved dry deciduous tree	20	1.8	1.5	0.1	5
BRCDt	Broadleaved cold deciduous tree	32	1.8	1.5	0.06	6
BREVs	Broadleaved evergreen shrub	27	1.6	1.1	0.06	6
NLEVt	Needleleaved evergreen tree	8	1.1	0.9	0.04	6
NLCDt	Needleleaved cold deciduous tree	22	1.7	1.5	0.04	6
C3GR	C_3 herbaceous (inc. crop)	27	1.8	1.3	0.06	6
C4GR	C_4 grass (inc. crop)	27	1.0	2	0.06	15
Moss	Bryophytes	61	2.6	1	∞	∞
Mean	(non-moss C_3)	20.8	1.6	1.2	0.065	5.75

/ISLSCP2_1/data/vegetation/edc_landcover_xdeg/ on 17 July 2009. The SiB2 15 class land cover classification has the greatest correspondence with the GPT classification of Hybrid6.5. These data were supplemented with information concerning tropical vegetation in the IGBP DISCover classification, and temperatures in the CRU climate dataset (see below), to create a merged product. The mapping used between the original datasets and Hybrid cover/GPTs is described in Table 2.

Leaf area: The LAI product derived from measurements made by NASA's Moderate Resolution Imaging Spectroradiometer instrument, flying aboard the Terra (EOS AM) satellite (http://modis.gsfc.nasa.gov/), was used to prescribe the global distribution of mean-monthly leaf area. Specifically, the Collection 5 MOD_BU 4 km dataset, described by Gao *et al.* (2008), and downloaded from ftp://primavera.bu.edu/pub/datasets/MODIS/MOD15_BU/C5/LAI/data/monthly/4km/ on 1 July 2009, was used. This 4 km product was degraded to QD resolution by simple averaging over land grid boxes, and then averaged for each month over calendar years 2001–2006.

Available water storage capacity: The global distribution of available water storage capacity per unit of soil depth was derived from the FAO *et al.* (2009) Harmonized World Soil Database (version 1.1). One of seven available water storage capacity (AWC) classes is assigned to each of the soil mapping units in the database, which are gridded globally at a resolution of 30 arc-seconds by 30 arc-seconds (about 1 km square). The global field of AWC was created and degraded to QD resolution by simple averaging over grid boxes of non-zero values of AWC. If a QD grid box contained no non-zero AWC soil units, but contained LAI in the MODIS derived product, a nominal AWC value of 100 mm m^{-1} was assigned to the land cover in that box.

AWC is taken to be the amount of water that can be held in the rooting zone between plant wilting point and field capacity (FC). There is a fairly linear relationship between FC and AWC across soil textual classes, and therefore Hybrid6.5 converts AWC to field capacity for internal hydrological calculations by simple scaling. A scaling factor of 1.75 is used for the baseline simulations, a value at the lower end of the observed range.

Climate: Annual values of monthly precipitation, number of wet days, mean 24 h maximum and minimum temperatures, and mean vapour pressure at 0.5×0.5° resolution for calendar years 2001–2006 were obtained from the Climatic Research Unit, University of East Anglia TS 3.0 dataset (CRU, 2008). This product was derived by interpolating station meteorological data and is an update of the dataset described by Mitchell and Jones (2005). Mean-monthly values were calculated and then re-sampled to QD resolution.

Shortwave radiation was taken from the ISCCP-FD RadFlux version dataset (Zhang *et al.*, 2004; downloaded from ftp://isccp.giss.nasa.gov/outgoing/FLUX/MPF/ on 7 January 2009). These data were derived using the NASA Goddard Institute for Space Studies radiative transfer

Table 2. Land cover classification dataset mapping to Hybrid6.5 cover/GPT types

The SiB Model Class 'Ground cover with trees and shrubs' covers most savanna vegetation types, and so was further split using the IGBP savanna sub-divisions which distinguish degree of woodiness. In addition, herbaceous types are split into C_3 and C_4 physiologies based on annual maximum mean-monthly 24 h maximum temperature (obtained from the CRU climate forcing), with C_4 assumed when this is greater than 31 °C (based on the simulated vegetation distribution of Woodward *et al.*, 2004). GPT mnemonics are defined in Table 1.

SiB model class	IGBP land cover	Hybrid6.5 Cover/GPT
Water bodies		No vegetation
Evergreen broadleaf trees		BREVt
Broadleaf deciduous trees		BRCDt
Deciduous and evergreen trees		50% BRCDt; 50% NLEVt
Evergreen needleleaf trees		NLEVt
Deciduous needleleaf trees		NLCDt
Ground cover with trees and shrubs		BREVs if Woody Savannas + Savannas=0
	Woody savannas (30–60% forest canopy cover)	45% BRDDt; 55% herbaceous
	Savannas (10–30% forest canopy cover)	20% BRDDt; 80% herbaceous
Groundcover only		Herbaceous
Broadleaf shrubs with perennial ground cover		50% BREVs; 50% herbaceous
Broadleaf shrubs with bare soil		BREVs
Groundcover with dwarf trees and shrubs		50% BREVs; 50% herbaceous
Bare soil		No vegetation
Agricultural or C_3 grassland		Herbaceous
Persistent wetland		Moss
Ice cap and glacier		No vegetation
Missing data		No vegetation

model and ISCCP cloud climatology and ancillary datasets. Monthly mean surface downwelling full sky shortwave (i.e. 0.2–5.0 μm) over 2001–2006 was calculated, and downscaled from its native 2.5×2.5° resolution to 0.25×0.25° by simple re-sampling.

Atmospheric CO_2: The global surface concentration of atmospheric CO_2 is prescribed to be 375.7 ppm, which is the mean of the global marine surface annual means measured during calendar years 2001–2006 by the NOAA ESRL network (Conway *et al.*, 1994; Masarie and Tans, 1995; http://www.esrl.noaa.gov/gmd/ccgg/trends/).

Masking: All global fields were gridded to the same QD resolution, as explained above. Re-sampling the CRU climate fields resulted in 2310 out of 250 999 QD grid boxes with land but no climate data, and so these were not used in the simulations reported here. 1507 grid boxes had climate data and non-zero leaf area in the MODIS product, but no land in the FAO product. These grid boxes were assigned nominal AWC values of 100 mm m^{-1}.

Forcing climate data for 2090s simulations

In order to assess the potential sensitivity of the distribution of global plant production to an estimate of future climate, a typical GCM prediction for the end of this century was downloaded and formatted for input to Hybrid6.5. The GISS-AOM GCM (Russell *et al.*, 1995) Special Report on Emission Scenarios (SRES) A1B simulation was prepared for the IPCC AR4 (as a component of the 'WCRP CMIP3 multi-model dataset'). This simulation consisted of an initialization for preindustrial conditions, a run up to 2000 using observed radiative forcing, and then a run to 2100 using the A1B scenario of future radiative forcing. Monthly model output from 'Run 1' was downloaded from the IPCC-Model Output archive of the PCMDI on 5 August 2009 (https://esg.llnl.gov:8443/index.jsp). SRES A1B consists of a fairly rapid increase in anthropogenic greenhouse gas forcing, with atmospheric CO_2 concentrations rising rapidly to reach 720 ppm in calendar year 2100.

Monthly mean global surface fields for calendar years 2000–2100 of predicted precipitation rate, daily minimum and maximum temperatures, specific humidity, atmospheric pressure, and downwelling shortwave radiation were downloaded in the native spatial resolution of 4° longitude × 3° latitude and then re-sampled to the QD resolution. Monthly means of water vapour pressure were calculated from specific humidity and pressure, and mean-monthly anomalies of water vapour pressure, 24 h minimum and maximum temperatures, precipitation, and radiation between the decade 2091–2100 and the decade 2001–2010 were then calculated. These anomalies were then added to the observed mean-monthly values of these variables over calendar years 2000–2006 to create a future climate forcing dataset. If, after applying the anomaly, a given monthly radiation flux, rate of precipitation, or water vapour pressure were negative, the value was set to zero. Number of wet days per month and all non-climate forcings were not changed, except for atmospheric CO_2 concentration, which was set to 720 ppm.

Global mean temperature over QD land grid boxes is predicted to increase 2.1 K over the rest of this century, with much larger increases at high latitudes, especially in northern Eurasia where warming over 10 K is common. The Mediterranean region experiences strong drying, with reductions in mean annual rainfall of over 1 mm d^{-1} in many parts, such as much of Spain and Greece. Large parts of southern Africa also experience strong drying. Large increases in rainfall occur over southern Asia, especially Indonesia. Changes in mean annual radiation are relatively modest, with reductions over most high latitude regions and the Tibetan Plateau of up to 10 W m^{-2}, and increases over the Mediterranean region and parts of China. Atmospheric water vapour increases strongly over the tropics and eastern North America, with gains of over 300 Pa across India.

Results and discussion

Baseline simulation

A baseline simulation was performed using the constrained implementation of Hybrid6.5 described above, with initial ground temperatures set to the local January mean air temperature and initial relative soil water in each layer set to 0.8. Predicted NPP took about 30 years to reach quasi-equilibrium (i.e. no systematic long-term drift in any regions) under forcing with mean 2001–2006 conditions. A mean global value of 58.8 Pg C yr^{-1} was obtained over model years 35–45 (SIM1, Table 3). The predicted global distribution of this NPP is shown in Fig. 2, with the latitudinal distribution shown in Fig. 3 and global values for each GPT given in Table 3. The main drivers of the simulated spatial variability are precipitation, leaf area, growing season length, and the distribution of C_3 versus C_4 plants.

Predicted global NPP is similar to previous estimates, including those of Ajtay *et al.* (1979; 59.9 Pg C yr^{-1}) and Saugier *et al.* (2001; 62.6 Pg C yr^{-1}). The often cited value of 56.4 Pg C yr^{-1} of Field *et al.* (1998) (F98) is close to the Hybrid6.5 value, despite being based on much simpler algorithms (i.e. the CASA production efficiency model constrained by satellite measurements of light absorption). The slight difference with their value might be explained by the different (earlier) time period of their forcing (i.e. calendar years 1982–1990). However, comparison of values for individual GPTs (Table 3) indicates much greater differences between the model approaches than suggested by the global values and latitudinal distributions (Fig. 3) alone. In particular, Hybrid6.5 simulates 3.0 Pg C yr^{-1} (17.0%) lower NPP by broadleaved evergreen trees than reported in F98, which is compensated in the global value by higher NPP in all other GPTS, particularly C_4 grasses (+2.0 Pg C yr^{-1}, or 15.9% higher) and needleleaved evergreen trees (+1.1 Pg C yr^{-1}, or 23.2% higher).

Table 3. Distribution of NPP over GPTs as predicted by the Hybrid6.5 baseline simulation for modern conditions of climate, CO_2, and leaf area (SIM1)

Results also given for baseline conditions but constant maximum LAI (SIM2), fixed T_o (SIM3), equal physiological parameters across all GPTs (SIM4), 2090s climate and atmospheric CO_2 forcing (SIM5), and 2090s climate forcing only (SIM6). Also shown are NPP estimates for modern conditions derived from Field *et al.* (1998; F98), assuming that their 'Tropical rainforests'=BREVt; 'Broadleaf deciduous forests'=BRCDt; 'Broadleaf and needleleaf forests'=0.5×BRCDt + 0.5×NLEVt; 'Needleleaf evergreen forests'=NLEVt; 'Needleleaf deciduous forest'=NLCDt; 'Savannas'=0.77×C4GR+0.23×BRDD (ratio from this study); 'Perennial grasslands'=C3GR; 'Broadleaf shrubs'=BREVs; 'Tundra'=BREVs; 'Desert'=BREVs; and 'Cultivation'=C3GR. Mnemonics are defined in Table 1.

	BREVt	BRDDt	BRCDt	BREVs	NLEVt	NLCDt	C3GR	C4GR	Moss	Total	
SIM1	14.8	4.4	3.3	3.0	5.8	1.7	10.7	14.9	0.1	58.8	Pg C yr^{-1}
SIM2	15.9	5.4	4.4	3.6	7.2	2.4	14.2	18.6	0.2	71.9	Pg C yr^{-1}
SIM3	14.8	4.3	3.2	2.8	5.6	1.6	10.3	14.6	0.1	57.3	Pg C yr^{-1}
SIM4	14.3	3.6	3.4	3.8	4.5	1.5	11.0	8.1	0.3	50.5	Pg C yr^{-1}
SIM5	21.5	6.6	4.9	4.5	8.5	2.5	16.1	15.8	0.2	80.7	Pg C yr^{-1}
SIM6	14.0	4.2	3.3	2.9	5.8	1.8	10.5	14.7	0.1	57.3	Pg C yr^{-1}
F98	17.8	3.9	3.0	2.3	4.7	1.4	10.4	12.9	–	56.4	Pg C yr^{-1}

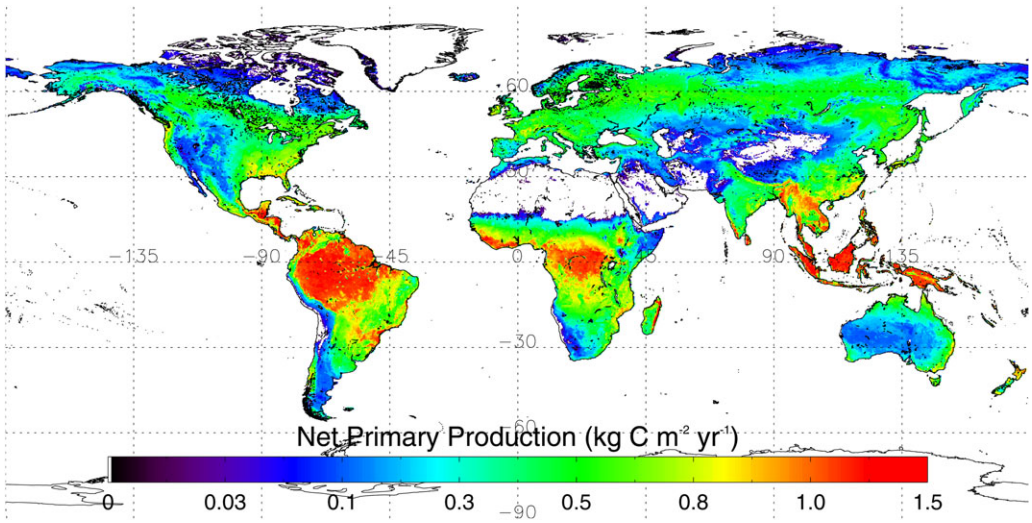

Fig. 2. Global distribution of NPP simulated by Hybrid6.5 under modern conditions (SIM1). Inputs are mean-monthly climate, leaf area, and atmospheric CO_2 concentration for calendar years 2001–2006, vegetation distribution from calendar years 1992–1993, and soil properties from a merged dataset of the most recent measurements available. Total NPP=58.8 Pg C yr^{-1}, with the contribution from different GPTs given in Table 3.

The 17% lower NPP of the broadleaved evergreen tree GPT than in F98 is possibly due to the leaf-level photosynthesis approach in Hybrid6.5. Consideration of light extinction over chloroplasts introduces a strong constraint on leaf and canopy photosynthesis at high light levels. In contrast, the CASA approach (Potter *et al.*, 1993) uses a light-use efficiency (LUE) algorithm in which monthly production is calculated as a linear function of absorbed light, modified by temperature and soil moisture scalars. The high LAI of tropical rainforests ensures that most of the incident light is absorbed, and the wet and warm conditions ensure that most of this energy is converted into fixed C. However, observations indicate that canopy photosynthesis does not scale linearly with incident light, even on monthly timescales. For example, Malhi *et al.* (1998) measured canopy photosynthesis light response curves with the eddy covariance technique at a productive tropical rainforest site in central Amazonia. Canopy photosynthesis exhibited strong non-linearity, and saturated completely at solar radiation >600 W m^{-2}, suggesting that, at least qualitatively, the light response approach of Hybrid6.5 is more realistic than the approach of CASA.

Clark *et al.* (2001) critically analysed tropical forest NPP field data, and after excluding a discredited outlier, reported a maximum upper NPP bound in tropical old-growth forest of 2170 g C m^{-2} yr^{-1}, close to the Hybrid6.5 maximum for broadleaved evergreen trees of 2311 g C m^{-2} yr^{-1}. Measuring NPP in the field, especially in tropical rainforests, is notoriously difficult, and therefore comparisons with field data should be made cautiously, but this close match is encouraging. The predicted mean value of 1152 g C m^{-2} yr^{-1} is perhaps harder to evaluate as this would require a comprehensive measurement campaign across the global tropics. Nevertheless, it is again encouraging that the mean value of upper bound estimates for old growth

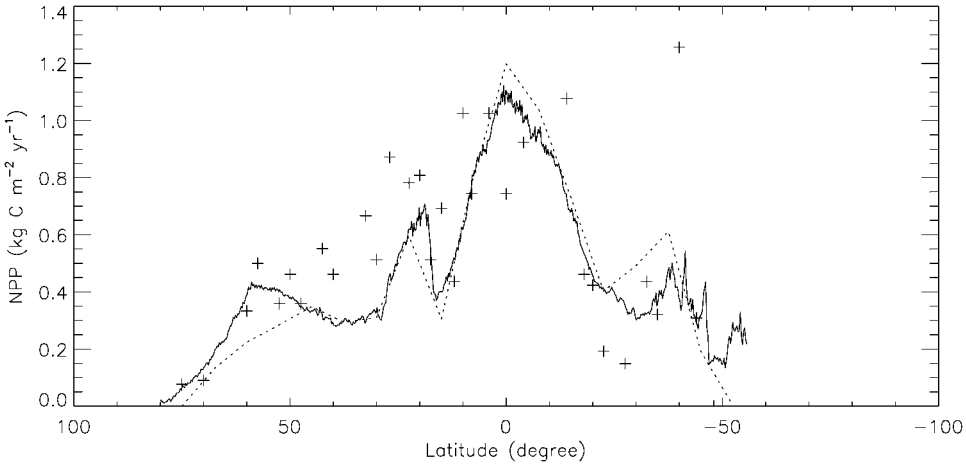

Fig. 3. Latitudinal distribution of modern mean NPP simulated by Hybrid6.5 (SIM1; solid line; mean for each 0.25° latitudinal band). Also shown are observations compiled by Zaks *et al.* (2007) (crosses; binned into 2.5° bands), and the simulation results of Field *et al.* (1998) (dotted line).

tropical forests reported by Clark *et al.* (2001) is 1248 g C m^{-2} yr^{-1}, close to the Hybrid6.5 global mean estimate.

The 16% higher NPP of C_4 grasses in Hybrid6.5 than in F98 is presumably at least partly a result of the use of a globally constant light use efficient in CASA, whereas in reality light use efficiencies of C_3 and C_4 plants have very different temperature response functions (Ehleringer and Cerling, 2001).

The 23% higher needleleaved evergreen tree NPP in Hybrid6.5 than in F98 likely reflects an underestimation in F98. Figure 3 shows binned 2.5° band *in situ* observations compiled by Zaks *et al.* (2007) along with the predictions of the two models. These indicate that the Hybrid6.5 predictions are in line with observations at high northern latitudes, whereas the F98 values are perhaps too low. However, a rigorous quantitative comparison is not yet possible given the sampling distribution of the observations (Zaks *et al.*, 2007).

In addition to parameter values for different GPTs, other model assumptions could be responsible for differences between predicted and observed NPP. In particular, autotrophic respiration is modelled in Hybrid6.5 using a rather simple substrate-limited parameterization (Equation 7), calibrated such that 50% of fixed carbon is lost by this process over the long term. Theoretical evidence supports the idea of a relatively fixed ratio of NPP to GPP (Dewar, 2000), but *in situ* measurements of the components of NPP are too uncertain to assess model assumptions and predictions quantitatively. For example, Malhi *et al.* (2009) calculated NPP/GPP ratios for three intensively measured tropical rainforest sites in Amazonia, finding ratios of 0.32±0.07 at Caxiuaña, 0.34±0.10 at Manaus, and 0.49±0.16 at Tapajós. While these differences between sites were not statistically significant, they do suggest that the mean fraction of GPP lost to respiration is closer to 0.6 than 0.5 in this ecosystem type.

There is clearly a significant need for better observational constraints on NPP, both in terms of coverage and methodology. Inevitably, it is extremely challenging to measure all components of an ecosystem's carbon balance, especially those below-ground. Eddy covariance measurements over different vegetation types have increased our understanding of the relationships between atmospheric forcings, plant types, and carbon fluxes, but significant technological challenges remain in balancing integrated fluxes to the atmosphere with changes in stocks (e.g. Kominami *et al.*, 2008). Moreover, recent evidence such as that of substantial internal recycling of respired carbon through root-canopy transport (Aubrey and Teskey, 2009), suggests that links between physiology and fluxes may be more difficult to determine from atmospheric measurements than previously appreciated.

Despite these caveats, it is reasonable to conclude that Hybrid6.5 predicts realistic NPP values across different GPTs and climate systems.

Sensitivity tests

A mechanistic model such as Hybrid6.5 can be used to address a wide variety of questions concerning plant production, including the impact of different processes and their parameterizations on model outcomes. Interesting questions include the relationships between the timing of leaf display and production, consequences of acclimative processes, and the significance of physiological differences between plant types. Answers to these questions can improve our understanding of actual processes, inform model development, and structure further experimental research. Three model sensitivity experiments designed with these points in mind are described and evaluated below.

Leaf phenology: The relative extent to which parameterization of leaf phenological processes influences model outcomes compared to other components is unclear. To address this question, the last 10 years of the baseline simulation were repeated except that LAI in each grid box was held constant at its maximum mean-monthly value over 2001–2006. The difference between this predicted NPP and

that predicted in the baseline simulation is therefore a measure of the extent to which leaf area variation between seasons influences plant production. The results of this simulation are shown for each GPT in Table 3 (SIM2), with the geographical distributions of the absolute and relative differences shown in Fig. 4.

Large absolute effects of phenology occur for grass and cropland production and are located in the Prairie Belt of North America, the Sahel, Chinese croplands, and the Indian sub-continent (Fig. 4A). These results are interesting in that they suggest that leaf area duration is sub-optimal for annual food production in these regions, and that soil moisture may not be the major control on phenology. Cropland phenology is dominated by planting time, developmental rates, and harvesting schedules, whereas savanna leaf area may be limited by fire in many years. It is possible that constraints not included in these simulations, such as nutrient supply, limit leaf area duration in these regions. However, to understand further the significance of this result for grass and cropland production, it will be necessary to conduct careful site-level model-data comparisons over the full seasonal cycle.

Forcing LAI to its annual maximum increases global NPP by 22.3%, with the greatest relative increases in moss (42.9%) and needleleaved cold deciduous trees (38.7%) (Table 3). Large relative increases are evident in tundra ecosystems and central Asian croplands (Fig. 4B). It is to be expected that plants growing in regions with very cold winters will be strongly influenced by their phenology, although the magnitude of the effect in needleleaved cold deciduous trees across North America and parts of northern Asia is surprisingly high. These results suggest that correctly simulating the phenology of *Larix* spp. and croplands needs to be a priority in the future development of dynamic vegetation models.

Temperature acclimation: In order to assess the significance of acclimation processes for annual plant production, the last 10 years of the baseline simulation were repeated but with the optimum temperature for chloroplast electron transport (T_o, Equation 3) held constant at 31 °C. The

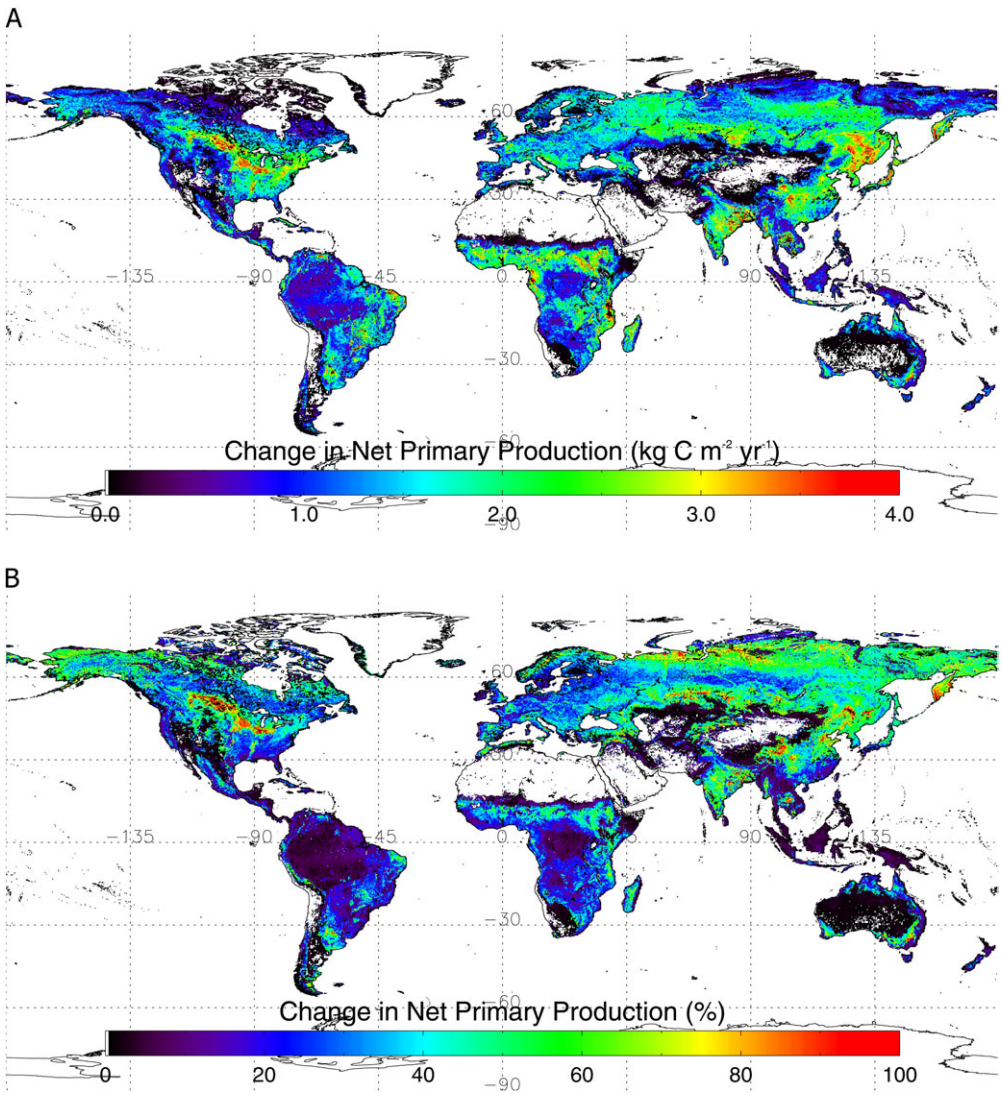

Fig. 4. Simulated absolute (A) and relative (B) effect on NPP of maintaining LAI at the maximum observed mean-monthly value in each 0.25° grid box (SIM2, Table 3).

global effect is a small (2.52%) reduction in NPP (Table 3, SIM3), suggesting that acclimation of T_o is not very important for plant production at the global scale. However, the parameterization used was optimized for conditions in Pennsylvania, USA, and regions cooler than this location exhibit reductions in NPP of up to 20% when T_o is held constant, whereas warmer regions exhibit modest (i.e. <50 g C m^{-2} yr^{-1}) increases. This suggests that the parameterization of temperature acclimation needs to be made GPT and/or location-specific. Also, it is possible that photosynthetic temperature acclimation processes are indeed more important than suggested here. Full acclimation probably involves changes in a number of chloroplast biochemical properties in addition to electron transport (Hikosaka *et al.*, 2006).

Physiological parameters: An ongoing debate in the development of dynamic global vegetation models concerns the level of physiological differences between plant types that need to be included to capture the range of potential plant responses to environmental forcing (Lavorel *et al.*, 2007). As a contribution to that debate, the last 10 years of the baseline simulation were repeated but with all GPTs assigned parameter values equal to the mean values of the non-moss C_3 GPTs (Table 1). Differences between this simulation and the baseline simulation quantify the importance of GPT-specific parameterizations for plant production processes.

Mean global NPP is reduced by 14.1%, mainly as a result of the lack of C_4 physiology (Table 3, SIM4). Within C_3 GPTs (excluding mosses), NPP changes by between –22.3% (NLEVt) and +27.9% (BREVs), a large range. These effects are primarily due to the amount of photosynthetic N per unit ground area being controlled by specific leaf area, foliage N content, and relative photosynthetic capacity (Table 1). This suggests that a thorough understanding of the variation in these parameters within and between GPTs would have significant benefits for our ability to model global plant production. Efforts are currently underway to address this issue through the joint IGBP-DIVERSITAS Fast-Track Initiative (http://www.igbp.net/page.php?pid=369).

Climate change simulations

Applying the climate change anomalies predicted by the GISS-AOM GCM under the A1B emissions scenario for the 2090s to observed modern climate, and with atmospheric CO_2 increased from 375.7 ppm to 720 ppm, results in a 37.3% increase in global NPP to 80.7 Pg C yr^{-1} (Table 3, SIM5). Figure 5 shows the global distributions of the absolute and relative effects of climate and CO_2 change on NPP, with values for individual GPTs given in Table 3. The relative change is fairly consistent across C_3 plant types, ranging from +42.9% for moss to +52.9% for broadleaved evergreen shrubs. By contrast, NPP is only increased by 5.9% in C_4 grass and cropland. The major response of NPP comes from the stimulation of C_3 photosynthesis by atmospheric CO_2, with the largest absolute increases occurring in tropical rainforests (i.e. +6.7 Pg C yr^{-1} for broadleaved evergreen trees) and C_3 grass and croplands (i.e. +5.5 Pg C yr^{-1}) (Fig. 5A; Table 3).

The broad patterns in the spatial distribution of the absolute effects of climate change and increasing atmospheric CO_2 on NPP (Fig. 5A) are related to the distribution of baseline C_3 production. By contrast, the distribution of the relative effect (Fig. 5B) is dominated by the distribution of C_4 plants, plus the pattern of precipitation anomalies. Despite the general stimulation of NPP, parts of India experience reductions due to the combination of C_4 physiology and reduced radiation.

The response of NPP to climate change alone was tested by re-running SIM5, but with atmospheric CO_2 held at 375.7 ppm. Global NPP was reduced compared to the 2001–2006 baseline simulation by 2.5% (Table 3, SIM6), although with significant spatial variation (Fig. 6). The largest relative impacts of climate change alone are over southern Africa, central Australia, northern Mexico, and the Mediterranean region, where reductions in NPP of over 20% are common. Absolute reductions of NPP are greatest in South American tropical rainforests, southern Africa, and the Mediterranean region. Climate change alone is predicted to have modest positive impacts on boreal forest production (needleleaved evergreen and needleleaved cold deciduous tree GPTs in Table 3), as well as significant positive impacts on tundra vegetation at high latitudes and on the Tibetan Plateau (Fig. 6B).

While these climate change predictions are fairly typical, it needs to be borne in mind that the simulations presented here use predictions from just one climate model forced with just one particular emissions scenario.

To what extent can we believe these large positive effects of CO_2 fertilization on NPP, and what will happen to this additional production? Norby *et al.* (2005) reviewed experimental evidence concerning forest ecosystem NPP responses to increased atmospheric CO_2. They concluded that NPP is stimulated by a median of 23±2% for a CO_2 increase of ≈376 to ≈550 ppm. Linear extrapolation of this relationship gives an increase in NPP of 45.5% at 720 ppm, close to the predictions for C_3 GPTs presented here. However, acclimative processes and ecosystem feedbacks may act to change the future response to CO_2, whereas these simulations assume unchanging leaf photosynthetic capacity and leaf area. Future leaf N and/or area may decrease in response to progressive N limitation (Luo *et al.*, 2004), whereas increased soil N mineralization at higher temperatures may reduce or negate this effect (Melillo *et al.*, 2002). Increased soil water levels through stomatal closure may increase leaf area, and so increase the relative response to future CO_2 levels. The balance of these opposing effects will probably differ significantly between regions and plant types and can be addressed using the fully dynamic implementation of the Hybrid6.5 model.

It is important to consider the fate of any additional future production. If the main effect is increased growth of short-lived tissue, such as fine roots (as is believed to occur in elevated CO_2 experimental studies such as that of Norby *et al.*, 2002), then the gains in NPP may not impact plant

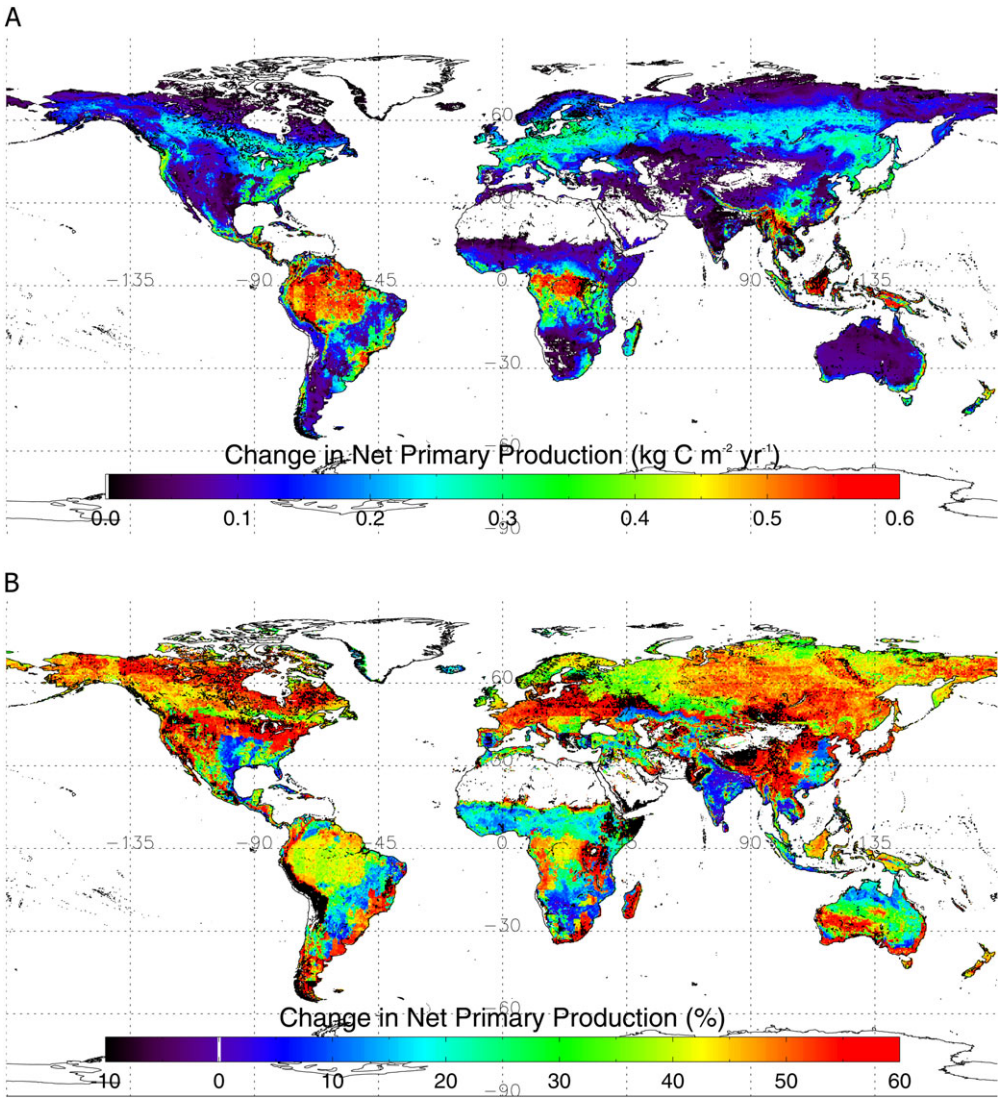

Fig. 5. Simulated absolute (A) and relative (B) effect of climate change predicted by the GISS-AOM GCM under the A1B emissions scenario and CO_2 increase (from 375.7 to 720 ppm) on NPP between 2001–2010 and 2091–2100. Global NPP is increased by 37.3% (SIM5, Table 3).

growth and food production (although below-ground metabolism will be affected). Other factors will probably also influence the future response of NPP at regional scales, including land use change, stand dynamics, disease, pollution, and the effects of temperature extremes. Respiration may respond to increased CO_2 in ways not predicted by the simple approach used here (e.g. Leakey *et al.*, 2009), although current understanding of respiration processes limits our ability to construct mechanistic models with the same level of detail as for photosynthesis.

Conclusions

Although observations provide only limited constraints, they suggest that Hybrid6.5 is capable of predicting the global distribution of NPP at least as well as previous approaches, and does so from an improved understanding of leaf-level physiology. The large predicted increase in future tropical rainforest NPP suggests that this ecosystem type could play a major role in limiting future atmospheric CO_2 levels. A major concern is the predicted large negative impact of climate change on primary production throughout southern Africa and the Mediterranean region. The capacity for CO_2 fertilization of photosynthesis to provide increased future food production, and its impact on ecosystem processes, need to be carefully assessed through further model development and sensitivity testing.

Improvements in the predictive abilities of dynamic global vegetation models will come about through a range of activities. The simulations presented here suggest that the following will be of particular value: (i) characterization of spatial and taxonomic variability in basic physiological parameters (such as those listed in Table 1); (ii) incorporation of acclimative processes in models; (iii) attention to phenological processes in needleleaved deciduous trees and croplands; (iv) improved observational

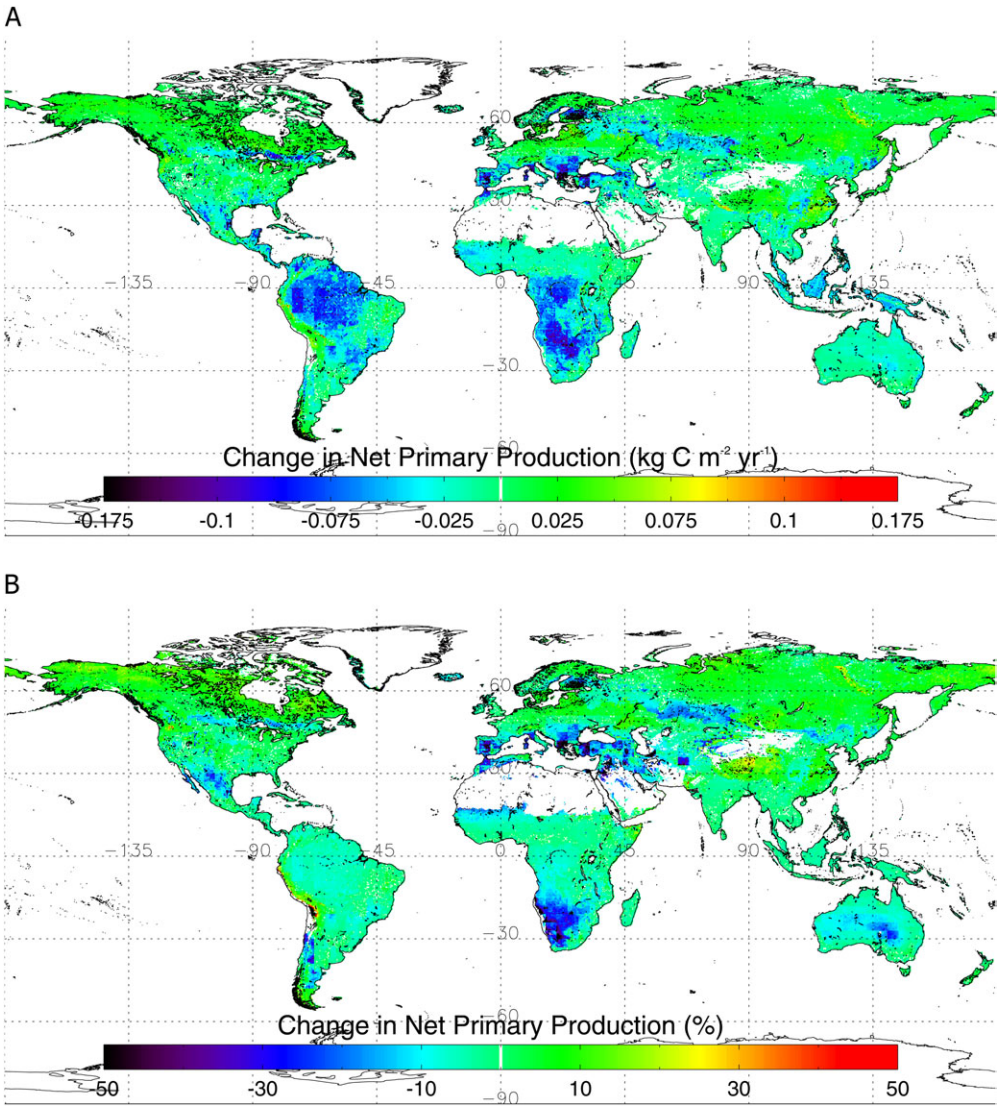

Fig. 6. As Fig. 5, except atmospheric CO_2 held at current levels (i.e. 375.7 ppm). Global NPP falls by 2.5% (SIM6, Table 3) compared to under modern conditions.

datasets on ecosystem carbon flows and stocks; and (v) improved understanding of the physiology of carbon metabolism (especially respiration) and the influences of nutrient feedbacks. What is most pressing is that experimentalists and modellers work together to improve understanding and reduce uncertainties.

Acknowledgements

An invitation to the 4th European Plant Science Organization (EPSO) Conference 2008 in Toulon, France, provided the stimulation for the work presented here. I am extremely grateful to Sönke Zaehle for valuable discussions during the development of Hybrid6.5 and Marina Frolova-Walker for help with the quote by K. A. Timiryazev. I also thank Bill Rossow and Yuanchong Zhang (ISCCP, NASA GISS), Ian (Harry) Harris (CRU, UEA), and Ranga B Myneni and Arindam Samanta (Boston University) for making their data available and assistance with processing. The IDL routines written and made freely available by David Fanning (http://www.dfanning.com/) solved many data handling problems. Funding was provided by the CNRS (France), the European Commission through Contract MRTN-CT-2004-512464 (GREENCYCLES Marie Curie Research Training Network), and the CNRS/INSU (France) EC2CO programme.

References

Ajtay GL, Ketner P, Duvigneaud P. 1979. Terrestrial primary productivity and phytomass. In: Bolin B, Degens ET, Kempe S, Ketner P, eds. *The global carbon cycle, SCOPE 13*. New York, USA: John Wiley and Sons, 129–182.

Aubrey DP, Teskey RO. 2009. Root-derived CO_2 efflux via xylem stream rivals soil CO_2 efflux. *New Phytologist* **184,** 35–40.

Berry J, Björkman O. 1980. Photosynthetic response and adaptation to temperature in higher plants. *Annual Review of Plant Physiology* **31,** 491–543.

Berry JA, Farquhar GD. 1978. The CO_2 concentration function of C_4 photosynthesis: a biochemical model. In: Hall D, Coombs J, Goodwin

T, eds. *Proceedings of the 4th international congress on photosynthesis*. London: Biochemical Society, 119–131.

Bonan GB, Levis S, Sitch S, Vertenstein M, Oleson KW. 2003. A dynamic global vegetation model for use with climate models: concepts and description of simulated vegetation dynamics. *Global Change Biology* **9,** 1543–1566.

Bowling DR, Pataki DE, Randerson JT. 2008. Carbon isotopes in terrestrial ecosystem pools and CO_2 fluxes. *New Phytologist* **178,** 24–40.

von Caemmerer S, Farquhar GD. 1981. Some relationships between the biochemistry of photosynthesis and the gas exchange of leaves. *Planta* **153,** 376–387.

Clark DA, Brown S, Kicklighter DW, Chambers JQ, Thomlinson JR, Ni J, Holland EA. 2001. Net primary production in tropical forests: an evaluation and synthesis of existing field data. *Ecological Applications* **11,** 371–384.

Collatz GJ, Ball JT, Grivet C, Berry JA. 1991. Physiological and environmental regulation of stomatal conductance, photosynthesis and transpiration: a model that includes a laminar boundary layer. *Agricultural and Forest Meteorology* **54,** 107–136.

Collatz GJ, Ribas-Carbo M, Berry JA. 1992. Coupled photosynthesis-stomatal conductance model for leaves of C_4 plants. *Australian Journal of Plant Physiology* **19,** 519–538.

Conway TJ, Tans PP, Waterman LS, Thoning KW, Kitzis DR, Masarie KA, Zhang N. 1994. Evidence for interannual variability of the carbon cycle from the National Oceanic and Atmospheric Administration/ Climate Monitoring and Diagnostics Laboratory Global Air Sampling Network. *Journal of Geophysical Research* **99,** 22,831–22,855.

Cox PM. 2001. *Description of the 'TRIFFID' dynamic global vegetation model*. Hadley Centre Technical Note 24.

Cramer W, Kicklighter DW, Bondeau A, Moore III B, Churkina G, Nemry B, Ruimy A, Schloss AL. 1999. **(The Participants of the Potsdam NPP Model Intercomparison Project).** 1999. Comparing global models of terrestrial net primary productivity (NPP): overview and key results. *Global Change Biology* **5,** Supplement1–15.

CRU. 2008. University of East Anglia Climate Research Unit (CRU). *CRU datasets* British Atmospheric Data Centre, 2008, downloaded from http://badc.nerc.ac.uk/data/cru on 15/07/09.

Dewar RC. 2000. A model of the coupling between respiration, active processes and passive transport. *Annals of Botany* **86,** 279–286.

Ehleringer JR, Cerling TE. 2001. Photosynthetic pathways and climate. In: Schulze ED, Heimann M, Harrison SP, Holland EA, Lloyd J, Prentice IC, Schimel D, eds. *Global biogeochemical cycles in the climate system*. San Diego: Academic Press, 267–277.

FAO/IIASA/ISRIC/ISSCAS/JRC. 2009. *Harmonized World Soil Database (version 1.1)*. FAO, Rome, Italy and IIASA, Laxenburg, Austria.

Farquhar GD, von Caemmerer S, Berry JA. 1980. A biochemical model of photosynthetic CO_2 assimilation in leaves of C_3 species. *Planta* **149,** 78–90.

Field CB, Behrenfeld MJ, Randerson JT, Falkowski P. 1998. Primary production of the biosphere: integrating terrestrial and oceanic components. *Science* **281,** 237–240.

Forstreuter M. 1998. What can we learn from microcosms? In: Jarvis PG, ed. *European forests and global change: the likely impact of rising CO_2 and temperature*. Cambridge University Press, 274–292.

Friend AD. 1995. PGEN: an integrated model of leaf photosynthesis, transpiration, and conductance. *Ecological Modelling* **77,** 233–255.

Friend AD. 1998. Parameterization of a global daily weather generator for terrestrial ecosystem modelling. *Ecological Modelling* **109,** 121–140.

Friend AD. 2001. Modelling canopy CO_2 fluxes: are 'big-leaf' simplifications justified? *Global Ecology and Biogeography* **10,** 603–619.

Friend AD, Geider RJ, Behrenfeld MJ, Still CJ. 2009. Photosynthesis in Global-Scale Models. In: Laisk A, Nedbal V, Govindjee, eds. *Photosynthesis* in silico*: understanding complexity from molecules to ecosystems*. Springer Series, Advances in Photosynthesis and Respiration, Vol. 29. Dordrecht, The Netherlands: Springer, 465–497.

Friend AD, Kiang NY. 2005. Land surface model development for the GISS GCM: effects of improved canopy physiology on simulated climate. *Journal of Climate* **18,** 2883–2902.

Friend AD, White A. 2000. Evaluation and analysis of a dynamic terrestrial ecosystem model under preindustrial conditions at the global scale. *Global Biogeochemical Cycles* **14,** 1173–1190.

Gao F, Morisette JT, Wolfe RE, Ederer G, Pedelty J, Masuoka E, Myneni R, Tan B, Nightingale J. 2008. An algorithm to produce temporally and spatially continuous MODIS-LAI time series. *IEEE Geoscience and Remote Sensing Letters* **5,** 60–64.

Geng S, Auburn J, Brandstetter E, Li B. 1988. *A program to simulate meteorological variables: documentation for SIMMETEO*. University of California, Davis: Department of Agronomy and Range Science.

Gifford RM. 1995. Whole plant respiration and photosynthesis of wheat under increased CO_2 concentration and temperature: long-term vs. short-term distinctions for modelling. *Global Change Biology* **1,** 385–396.

Hansen J, Russell G, Rind D, Stone P, Lacis A, Lebedeff S, Ruedy R, Travis L. 1983. Efficient three-dimensional global models for climate studies: Models I and II. *Monthly Weather Review* **111,** 609–662.

Harley PC, Thomas RB, Reynolds JF, Strain BR. 1992. Modelling photosynthesis of cotton grown in elevated CO_2. *Plant, Cell and Environment* **15,** 271–282.

Hikosaka K, Ishikawa K, Borjigidai A, Muller O, Onoda Y. 2006. Temperature acclimation of photosynthesis: mechanisms involved in the changes in temperature dependence of photosynthetic rate. *Journal of Experimental Botany* **57,** 291–302.

June T, Evans JR, Farquhar GD. 2004. A simple new equation for the reversible temperature dependence of photosynthetic electron transport: a study on soybean leaf. *Functional Plant Biology* **31,** 275–283.

Keenan T, García R, Friend AD, Zaehle S, Gracia C, Sabate S. 2009. Improved understanding of drought controls on seasonal variation in Mediterranean forest canopy CO_2 and water fluxes through combined *in situ* measurements and ecosystem modelling. *Biogeosciences* **6,** 1423–1444.

Kominami Y, Jomura M, Dannoura M, *et al*. 2008. Biometric and eddy-covariance-based estimates of carbon balance for a warm-temperate mixed forest in Japan. *Agricultural and Forest Meteorology* **148,** 723–737.

Kull O, Kruijt B. 1998. Leaf photosynthetic light response: a mechanistic model for scaling photosynthesis to leaves and canopies. *Functional Ecology* **12,** 767–777.

Lavorel S, Díaz S, Cornelissen JHC, Garnier E, Harrison SP, McIntyre S, Pausas JS, Pérez-Harguindeguy N, Roumet C, Urcelay C. 2007. Plant functional types: are we getting any closer to the Holy Grail? In: Canadell JG, Pataki D, Pitelka L, eds. *Terrestrial Ecosystems in a Changing World.* The IGBP Series. Berlin Heidelberg: Springer-Verlag, 149–164.

Leakey ADB, Xua F, Gillespie KM, McGrath JM, Ainsworth EA, Ort DR. 2009. Genomic basis for stimulated respiration by plants growing under elevated carbon dioxide. *Proceedings of the National Academy of Sciences, USA* **106,** 3597–3602.

Leith H. 1973. Primary production: terrestrial ecosystems. *Human Ecology* **1,** 303–332.

Loveland TR, Reed BC, Brown JF, Ohlen DO, Zhu J, Yang L, Merchant JW. 2000. Development of a global land cover characteristics database and IGBP DISCover from 1 km AVHRR data. *International Journal of Remote Sensing* **21,** 1303–1330.

Luo Y, Su B, Currie WS, *et al*. 2004. Progressive nitrogen limitation of ecosystem responses to rising atmospheric carbon dioxide. *Bioscience* **54,** 731–739.

Malhi Y, Nobre AD, Grace J, Kruijt B, Pereira MGP, Culf A, Scott S. 1998. Carbon dioxide transfer over a Central Amazonian rain forest. *Journal of Geophysical Research* **103,** 31,593–31,612.

Malhi Y, Aragão LEOC, Metcalfe DB, *et al*. 2009. Comprehensive assessment of carbon productivity, allocation and storage in three Amazonian forests. *Global Change Biology* **15,** 1255–1274.

Masarie KA, Tans PP. 1995. Extension and integration of atmospheric carbon dioxide data into a globally consistent measurement record. *Journal of Geophysical Research* **100,** 11,593–11,610.

Melillo JM, Steudler PA, Aber JD, Newkirk K, Lux H, Bowles FP, Catricala C, Magill A, Ahrens T, Morrisseau S. 2002. Soil warming and carbon-cycle feedbacks to the climate system. *Science* **298,** 2173–2176.

Mitchell TD, Jones PD. 2005. An improved method of constructing a database of monthly climate observations and associated high-resolution grids. *International Journal of Climatology* **25,** 693–712.

Norby RJ, Hanson PJ, O'Neill EG, *et al*. 2002. Net primary productivity of a CO_2-enriched forest and implications for carbon storage. *Ecological Applications* **12,** 1261–1266

Norby RJ, DeLucia EH, Gielen B, *et al*. 2005. Forest response to elevated CO_2 is conserved across a broad range of productivity. *Proceedings of the National Academy of Sciences, USA* **102,** 18,052–18,056.

Potter CS, Randerson JT, Field CB, Matson PA, Vitousek PM, Mooney HA, Klooster SA. 1993. Terrestrial ecosystem production: a process model based on global satellite and surface data. *Global Biogeochemical Cycles* **7,** 811–841.

Prince SD, Goward SN. 1995. Global primary production: a remote sensing approach. *Journal of Biogeography* **22,** 815–835.

Richardson CW, Wright DA. 1984. *WGEN: a model for generating daily weather variables*. US Department of Agriculture, Agricultural Research Service.

Russell GL, Miller JR, Rind D. 1995. A coupled atmosphere–ocean model for transient climate change studies. *Atmosphere–Ocean* **33,** 683–730.

Sands PJ. 1996. Modelling canopy production. III. Canopy light-utilisation efficiency and its sensitivity to physiological and environmental variables. *Australian Journal of Plant Physiology* **23,** 103–114.

Saugier B, Roy J, Mooney HA. 2001. Estimations of global terrestrial productivity: Converging towards a single number? In: Roy J, Saugier B, Mooney HA, eds. *Terrestrial Global Productivity*. San Diego, California, USA: Academic Press, 543–557.

Sellers PJ, Berry JA, Collatz GJ, Field CB, Hall FG. 1992. Canopy reflectance, photosynthesis, and transpiration. III. A reanalysis using improved leaf models and a new canopy integration scheme. *Remote Sensing of Environment* **42,** 187–216.

Sitch S, Smith B, Prentice IC, *et al*. 2003. Evaluation of ecosystem dynamics, plant geography and terrestrial carbon cycling in the LPJ dynamic global vegetation model. *Global Change Biology* **9,** 161–185.

Spitters CJT. 1986. Separating the diffuse and direct component of global radiation and its implications for modeling canopy photosynthesis Part II. Calculation of canopy photosynthesis. *Agricultural and Forest Meteorology* **38,** 231–242.

Spitters CJT, Toussaint HAJM, Goudriaan J. 1986. Separating the diffuse and direct component of global radiation and its implications for modeling canopy photosynthesis Part I. Components of incoming radiation. *Agricultural and Forest Meteorology* **38,** 217–229.

Veres JS, Williams III GJ. 1984. Time course of photosynthetic temperature acclimation in *Carex eleocharis* Bailey. *Plant, Cell and Environment* **7,** 545–547.

Woodward FI, Lomas MR, Kelly CK. 2004. Global climate and the distribution of plant biomes. *Philosophical Transactions of the Royal Society of London, Series B* **359,** 1465–1476.

Yamasaki T, Yamakawa T, Yamane Y, Koike H, Satoh K, Katoh S. 2002. Temperature acclimation of photosynthesis and related changes in photosystem II electron transport in winter wheat. *Plant Physiology* **128,** 1087–1097.

Zaehle S, Friend AD. 2010. Carbon and nitrogen cycle dynamics in the O–CN land surface model: I. Model description, site-scale evaluation, and sensitivity to parameter estimates. *Global Biogeochemical Cycles* **24,** GB1005, doi:10.1029/2009GB003521.

Zaks DPM, Ramankutty N, Barford CC, Foley JA. 2007. From Miami to Madison: Investigating the relationship between climate and terrestrial net primary production. *Global Biogeochemical Cycles* **21,** GB3004, doi:10.1029/2006GB002705.

Zhang Y, Rossow WB, Lacis AA, Oinas V, Mishchenko MI. 2004. Calculation of radiative fluxes from the surface to top of atmosphere based on ISCCP and other global data sets: Refinements of the radiative transfer model and the input data. *Journal of Geophysical Research* **109,** D19105, doi:10.1029/2003JD004457.